

Optimal Thermoelectricity with Quantum Spin Hall Edge States

Daniel Gresta,¹ Mariano Real,² and Liliana Arrachea¹

¹*International Center for Advanced Studies, ECyT-UNSAM, Campus Miguelete, 25 de Mayo y Francia, 1650 Buenos Aires, Argentina*

²*Instituto Nacional de Tecnología Industrial, INTI, Avenida General Paz 5445, 1650 Buenos Aires, Argentina*

 (Received 6 May 2019; revised manuscript received 16 September 2019; published 28 October 2019)

We study the thermoelectric properties of a Kramers pair of helical edge states of the quantum spin Hall effect coupled to a nanomagnet with a component of the magnetization perpendicular to the direction of the spin-orbit interaction of the host. We show that the transmission function of this structure has the desired qualities for optimal thermoelectric performance in the quantum coherent regime. For a single magnetic domain, there is a power generation close to the optimal bound. In a configuration with two magnetic domains with different orientations, pronounced peaks in the transmission functions and resonances lead to a high figure of merit. We provide estimates for the fabrication of this device with HgTe quantum-well topological insulators.

DOI: [10.1103/PhysRevLett.123.186801](https://doi.org/10.1103/PhysRevLett.123.186801)

Introduction.—Thermoelectricity in the quantum regime has attracted great interest for some years now [1,2]. Systems hosting edge states, like the quantum Hall and quantum spin Hall states, are paradigmatic realizations of quantum coherent transport. Several theoretical and experimental results on heat transport and thermoelectricity in these systems have recently been reported [3–31].

Unlike the quantum Hall state, which is generated by a strong magnetic field, the quantum spin Hall (QSH) state, taking place in two-dimensional (2D) topological insulators (TIs), preserves time-reversal invariance. Therefore, the edge states appear in helical Kramers pairs [32–37] with opposite spin orientations determined by the spin orbit of the TI. Several heat engines and refrigerators have recently been proposed, taking advantage of the fundamental chiral nature of the quantum Hall edge states, which manifests itself in multiple-terminal structures [19] and in quantum interference [20,21]. Recently, the property of charge fractionalization was also pointed out as a mechanism to enhance thermoelectricity [23]. All of these setups rely on the existence of quantum point contacts and quantum dots in the structure, tunnel coupled to the edge states, which are generated by recourse to constrictions. The fabrication of these elements is now normal in the context of the quantum Hall effect [38–40]. However, their realization in the context of the QSH effect has remained an experimental challenge so far [41], although they have been widely investigated theoretically [42–51].

In the quantum coherent regime, the electronic transport properties take place without inelastic scattering and are fully characterized by a transmission function. Particle-hole symmetry breaking is a necessary condition for steady-state heat to work conversion. Having transmission functions rapidly changing in energy within the relevant transport

window is the key to achieving optimal thermoelectricity [2,52–55]. The optimal performance is usually quantified by the *figure of merit* ZT , with the Carnot limit achieved for $ZT \rightarrow \infty$. This ideal limit can be realized for transmission functions containing δ -function-like peaks [52]. In this sense, structures with resonant levels like quantum dots are particularly promising [56–62]. On the other hand, electrical *power generation* out of heat is the aim of thermoelectric heat engines. This is optimized by transmission functions behaving like Heaviside- θ functions within the relevant transport window [54,55]. In the case of quantum Hall edge states, configurations with several quantum point contacts and quantum capacitors have recently been proposed to engineer the transmission function for optimal thermoelectricity by recourse to quantum interference [20].

In this Letter, we analyze a very different mechanism for edge-state thermoelectricity in a QSH structure. It is based on the coupling of a Kramers pair of helical edge states of the QSH to a magnetic domain. The structure we analyze is sketched in Fig. 1, where an edge-state pair of a 2D TI is

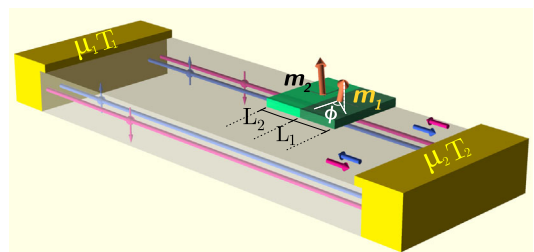


FIG. 1. Sketch of the setup scheme. 2D TIs contacted to Ohmic contacts at which a bias voltage $eV = \mu_1 - \mu_2$ and temperature difference $\Delta T = T_2 - T_1$ are applied. Two nanomagnets with magnetic moments \mathbf{m}_1 and \mathbf{m}_2 and lengths L_1 and L_2 are contacted to a helical Kramers pair of edge states.

contacted by nanomagnets. We consider two configurations, a single magnetic island with a given magnetic orientation, as well as two attached islands with different orientations of the magnetic moments. In both configurations, the key ingredient is a finite component of the magnetic moments perpendicular to the direction of the spin-orbit interaction of the TI. A similar structure was previously considered in Refs. [63–65], focusing on the interplay between spin-torque induced current and the consequent pumping induced by the precession of the magnetic moment. In combination to superconducting contacts, this structure has been investigated as a platform to realize topological superconductivity [66–68]. Here, we show that the simple two-terminal setup of Fig. 1, under the effect of simultaneous voltage and temperature biases, has the desired properties for optimal heat to electrical work dc conversion. We analyze the transmission function for this structure and the impact of its different features on the thermoelectric response. Remarkably, this function takes the best of the two worlds regarding power generation and large figure of merit, since it has features like a θ function and δ -function-type resonances due to bound states in the gap, as well as peaks like quantum dots. We provide estimates for the different components of the device, and we argue that it is within the state of the art of fabrication of 2D TI structures [35–37].

Thermoelectric performance in the quantum coherent regime.—We briefly review the linear-response thermoelectric approach assuming small differences of chemical potential $eV = \mu_1 - \mu_2$ (with $\mu_1 = \mu$), and temperature $\Delta T = T_2 - T_1$ (with $T_1 = T$), applied at the contacts of the edge states, as indicated in Fig. 1 [2]. The induced charge and heat currents are

$$\begin{pmatrix} I^C/e \\ I^Q \end{pmatrix} = \begin{pmatrix} \mathcal{L}_{11} & \mathcal{L}_{12} \\ \mathcal{L}_{21} & \mathcal{L}_{22} \end{pmatrix} \begin{pmatrix} X_1 \\ X_2 \end{pmatrix}. \quad (1)$$

We have introduced the affinities $X_1 = eV/k_B T$ and $X_2 = \Delta T/k_B T^2$. In the quantum coherent regime, the elements of the Onsager matrix are fully determined by the transmission function $\mathcal{T}(\varepsilon)$ as follows,

$$\mathcal{L}_{ij} = -T \int \frac{d\varepsilon}{h} \frac{\partial f(\varepsilon)}{\partial \varepsilon} (\varepsilon - \mu)^{i+j-2} \mathcal{T}(\varepsilon), \quad (2)$$

where $f(\varepsilon) = 1/(e^{(\varepsilon-\mu)/k_B T} + 1)$. The key for the thermoelectric heat to work conversion is encoded in the off-diagonal coefficient $\mathcal{L}_{12} = \mathcal{L}_{21}$. The quality of this conversion is evaluated in terms of the efficiency (for the heat engine), $\eta^{\text{he}} = (I^C T X_1)/I^Q$, with $P = I^C T X_1$ being the generated power, or coefficient of performance (for the refrigerator), $\eta^{\text{fri}} = -I^Q/I^C T X_1$, with $-I^Q$ being the heat current extracted from the cold reservoir. In both cases, for a given difference of temperature, the maximum values for

these coefficients can be parametrized by the figure of merit $ZT = \mathcal{L}_{21}^2/\text{Det}\hat{\mathcal{L}}$ as follows,

$$\eta^{\text{max}} = \eta_C^{\text{he/fri}} \frac{\sqrt{ZT+1}-1}{\sqrt{ZT+1}+1}, \quad (3)$$

with $\eta_C^{\text{he}} = [\eta_C^{\text{fri}}]^{-1} = \Delta T/T$ being the Carnot efficiency which is achieved for $ZT \rightarrow \infty$, while the value $\eta^{\text{he/fri}} \sim 0.3\eta_C$ corresponds to $ZT \sim 3$. As originally shown by Mahan and Sofo, the ideal upper bound $\eta_C^{\text{he/fri}}$ is obtained for $\mathcal{T}(\varepsilon) \sim \delta(\varepsilon - \varepsilon_0)$, while ZT attains high values when $\mathcal{T}(\varepsilon)$ has peaks within the relevant transport window $|\varepsilon - \varepsilon_0| \sim k_B T$. On the other hand, for the heat-engine operational mode, the maximum achievable power for a given ΔT and the corresponding efficiency are

$$P_{\text{max}} = \eta_C \frac{\mathcal{L}_{12}^2 X_2}{4\mathcal{L}_{11}}, \quad \eta(P_{\text{max}}) = \eta_C \frac{ZT}{2(ZT+2)}. \quad (4)$$

It has been shown that the maximum power is bounded by $0.32P_0$ for a transmission function of the form $\mathcal{T}(\varepsilon) \sim \theta(\varepsilon - \mu - \varepsilon_0)$, where $P_0 = (k_B \Delta T)^2/h$ [54].

Transmission function.—The structure sketched in Fig. 1 is modeled by the following Hamiltonian,

$$H = \int dx \Psi^\dagger(x) [(-i\hbar v_F \partial_x) \hat{\sigma}_z + \mathbf{Jm}(x) \cdot \hat{\boldsymbol{\sigma}}] \Psi(x), \quad (5)$$

where $\Psi(x) = (\psi_{R,\uparrow}(x), \psi_{L,\downarrow}(x))^T$, where we represent the right- (left-) moving electrons with velocity v_F and \uparrow (\downarrow) spin orientation, where \mathbf{J} is the magnetic exchange interaction between the magnetic moment of the island and the spin of the electrons, and where $\hat{\boldsymbol{\sigma}} = (\hat{\sigma}_x, \hat{\sigma}_y, \hat{\sigma}_z)$ are the Pauli matrices. The magnetic island is described by the following piecewise spatial distribution of the magnetic moment within segments of lengths $L_j = x_j - x_{j-1}$:

$$\mathbf{m}(x) = \sum_{j=1}^N \theta(x_j - x) \theta(x - x_{j-1}) \mathbf{m}_j. \quad (6)$$

$\mathbf{m}_j = (m_{j\perp} \cos\phi_j, m_{j\perp} \sin\phi_j, m_{j\parallel})$ is the magnetic moment per unit length with components $m_{j\parallel}$ (parallel) and $m_{j\perp}$ (perpendicular) with respect to the direction of the spin-orbit interaction of the TI. We focus on a single island ($N = 1$) and two islands ($N = 2$) of the same length, but with different orientations of the magnetic moment.

In order to calculate the transmission function, we proceed as in Ref. [69], starting from the evolution operator in space for the whole scattering region. It reads $\hat{\mathcal{U}}(x_N, x_0) = \prod_{j=1}^N \hat{\mathcal{U}}(x_j, x_{j-1})$, with

$$\begin{aligned}\hat{U}(x_j, x_{j-1}) &= \exp\left(i\frac{\varepsilon_{j\parallel}}{\hbar v_F}L_j\right) \exp\{-i\lambda_j \cdot \hat{\sigma}\} \\ &= \exp\left(i\frac{\varepsilon_{j\parallel}}{\hbar v_F}L_j\right) [\hat{\sigma}_0 \cos \lambda_j - i\mathbf{n}_j \cdot \hat{\sigma} \sin \lambda_j],\end{aligned}\quad (7)$$

$\lambda_j = (ie_{j\perp} \sin \phi_j, -ie_{j\perp} \cos \phi_j, \varepsilon)L_j/(\hbar v_F)$, with $e_{j\parallel,\perp} = Jm_{j\parallel,\perp}$, and $\mathbf{n}_j = \lambda_j/\lambda_j$. The transmission function is the inverse of the element 2,2 of the transfer matrix, which is, in turn, the inverse of the matrix $\hat{U}(L, 0)$. Hence, $\mathcal{T}(\varepsilon) = |\text{Det}[\hat{U}(x_N, x_0)]/\mathcal{U}(x_N, x_0)_{1,1}|^2$.

Single homogeneous island.—We start by discussing the case of a homogeneous domain of length L , described by the previous Hamiltonian with a single piece, $N = 1$. The resulting transmission function is

$$\mathcal{T}(\varepsilon) = \frac{|\varepsilon_{\perp}^2 - \varepsilon^2|}{|\varepsilon_{\perp}^2 - \varepsilon^2|\cos^2 \lambda + \varepsilon^2 \sin^2 \lambda}, \quad (8)$$

$\lambda = rl$, with $l = L/L_0$, $L_0 = \hbar v_F/\varepsilon_{\perp}$ and $r = \sqrt{(\varepsilon/\varepsilon_{\perp})^2 - 1}$. Notice that the transmission function depends not on the detailed orientation of the magnetic moment but on the projection m_{\perp} perpendicular to the direction of the spin-orbit interaction of the material. It is also symmetrical to $\varepsilon = 0$. The latter introduces an effective coupling between the two Kramers partners that may open a gap in the spectrum of magnitude ε_{\perp} .

The behavior of $\mathcal{T}(\varepsilon)$ is illustrated in Fig. 2, where we see its dependence on the length of the island. For short islands, there is a sizable tunneling amplitude through the magnetic island, while as the length of the magnet increases, the transmission function tends to a step function close to $\varepsilon \sim \varepsilon_{\perp}$. We get the following behavior of the transmission function at the opening of the gap as a function of length $\mathcal{T}(\varepsilon_{\perp}) = [1 + l^2]^{-1}$, with $l = L/L_0$, while the slope behaves as $d\mathcal{T}/d\varepsilon|_{\varepsilon_{\perp}} = 2l^4[1 + l^2]/3[1 + l^2]^3$, which saturates at the value of 2/3 for increasing l . For energies $\varepsilon > \varepsilon_{\perp}$, $\mathcal{T}(\varepsilon)$ exhibits oscillations with maxima $\mathcal{T}^{\max}(\varepsilon_n) = 1$ and minima $\mathcal{T}^{\min}(\varepsilon_m) = 1 - (\varepsilon_{\perp}/\varepsilon_m)^2$ at energies

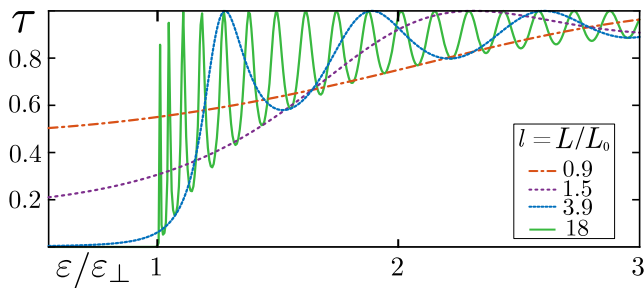


FIG. 2. Transmission function $\mathcal{T}(\varepsilon)$ defined in Eq. (8) within a range of lengths l for an island with homogeneous magnetic moment. Energies are expressed in units of $\varepsilon_{\perp} = Jm_{\perp}$, and lengths are expressed in units of $L_0 = \varepsilon_{\perp}/\hbar v_F$.

satisfying $(\varepsilon_{n(m)})^2 = (\varepsilon_{\perp})^2 + (\pi\alpha_{n(m)}\hbar v_F/L)^2$, with $\alpha_{n(m)}$ being an integer (half-integer) number, respectively.

The impact of the transmission function on the thermoelectric performance of the heat engine is illustrated in Fig. 3 for two lengths of the magnetic domain, in a range of chemical potentials close to the edge of the energy gap, within a temperature range scaled by the reference temperature $T_0 = \varepsilon_{\perp}/k_B$. For the shortest length shown in Figs. 3(a) and 3(b), $l = 10$, $\mathcal{T}(\varepsilon_{\perp}) < 0.01$, and $d\mathcal{T}/d\varepsilon|_{\varepsilon_{\perp}} \sim 0.65$, i.e., close to the maximal slope (2/3), implying a pronounced step in the transmission function at the closing of the energy gap. The plots shown in Figs. 3(c) and 3(d) correspond to a longer island of length $l = 20$, for which the step function is slightly more pronounced. For very low temperatures, within a scale $k_B T$ smaller than the width of the peaks of $\mathcal{T}(\varepsilon)$, both P_{\max} and ZT vanish for $\mu = \varepsilon_n$ [see the arrows in panels Figs. 3(a) and 3(b)]. As the temperature increases, the behavior of these quantities is ruled by the effect of several peaks. At sufficiently high temperatures, such that several maxima of $\mathcal{T}(\varepsilon)$ are included in an energy window of width $k_B T$, the behavior is dominated by the average between the envelopes for the minima and the maxima of $\mathcal{T}(\varepsilon)$. The resulting function is approximately a smoothed step function, independent of the length of the island. For this reason, P_{\max} shows a wide maximum centered at $\sim |\varepsilon_{\perp} - \mu| \sim k_B T$ [20,54]. The maximum is as high as $\sim 0.244P_0$, i.e., $\sim 75\%$ of the bound $0.32P_0$. $\mathcal{T}(\varepsilon)$ is symmetric with respect to $\varepsilon = 0$ and has a well of unit

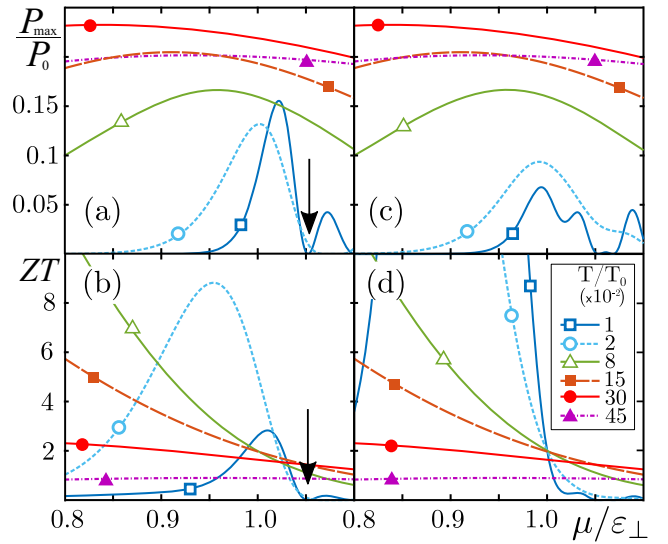


FIG. 3. (Upper panels) Maximum power and (lower panels) figure of merit ZT for a single magnetic domain of (a),(b) $l = 10$ and (c),(d) $l = 20$. The maximum values in (a) and (b) are (a) $P_{\max}(T = 0.3) = 0.240P_0$, (b) $ZT(T = 0.08) = 60$, (c) $P_{\max}(T = 0.45) = 0.244P_0$, and (d) $ZT(T = 0.02) = 274$. The temperatures are expressed in units of $T_0 = \varepsilon_{\perp}/k_B$, and the power is expressed in units of $P_0 = (k_B \Delta T)^2/h$. Other details are the same as in Fig. 2.

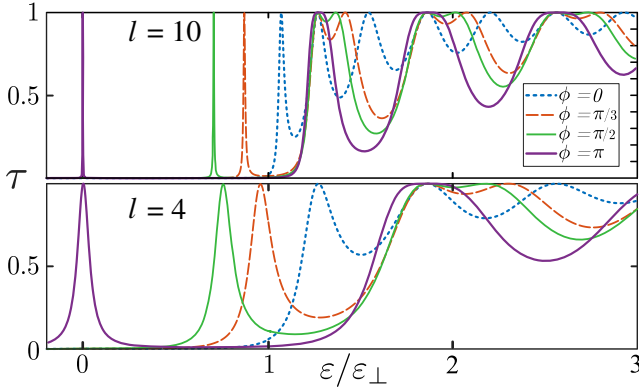


FIG. 4. Transmission function $\mathcal{T}(\varepsilon)$ defined in Eq. (8) for two magnetic domains of equal size ($l = 4, 10$), with the perpendicular component of the magnetic moments oriented with a relative tilt ϕ .

depth and width $\sim 2\varepsilon_{\perp}$. This feature dominates the behavior of the power and ZT at high temperatures. These properties depend mildly on the length of the island. Details of the effect of the different features of $\mathcal{T}(\varepsilon)$ on the thermoelectric response as a function of T are presented in the Supplemental Material [70].

Two domains.—We now turn to analyze the case where we have two pieces, corresponding to $N = 2$ in Eq. (7) with $L_1 = L_2 = L$, $\phi_1 = 0$, $\phi_2 = \phi$, and $\varepsilon_{\perp,1} = \varepsilon_{\perp,2} = \varepsilon_{\perp}$. The resulting transmission function reads

$$\mathcal{T}(\varepsilon) = \left\{ \left[\cos^2 \lambda + \frac{\sin^2 \lambda}{r^2} \left(\cos \phi - \frac{\varepsilon^2}{\varepsilon_{\perp}^2} \right) \right]^2 + \left[-\frac{\varepsilon \sin 2\lambda}{\varepsilon_{\perp} r} + \sin \phi \frac{\sin^2 \lambda}{r^2} \right]^2 \right\}^{-1}. \quad (9)$$

The new feature in the present case, in comparison to the case of a single magnetic moment, is the existence of resonances within the gap, $|\varepsilon| < \varepsilon_{\perp}$, for $\phi \neq 0$. The position of the resonant state depends on the phase difference ϕ . For $\phi = \pi$, Eq. (5) coincides in that case with the model introduced by Jackiw and Rebbi [71,72], which has a topological zero mode localized at the domain wall boundary. In the Supplemental Material [70], we analyze the impact of the length of the domains on the width of the resonant state. We also show that this feature is robust under weak disorder in the length of the domains and the orientation of the magnetization along each domain.

The behavior of the transmission function for two domains is illustrated in Fig. 4 for a set of orientations. The upper and lower panels show the transmission function for $l = 10$ and $l = 4$ for each domain, respectively. Note that the width of the resonance decreases for increasing l . The corresponding thermoelectric response is shown in Fig. 5. Close to the edge of the gap, the minima of $\mathcal{T}(\varepsilon)$ for $\phi = \pi$ are deeper than the ones for a single domain [see Eq. (6) of the Supplemental Material [70]]. Notice that the

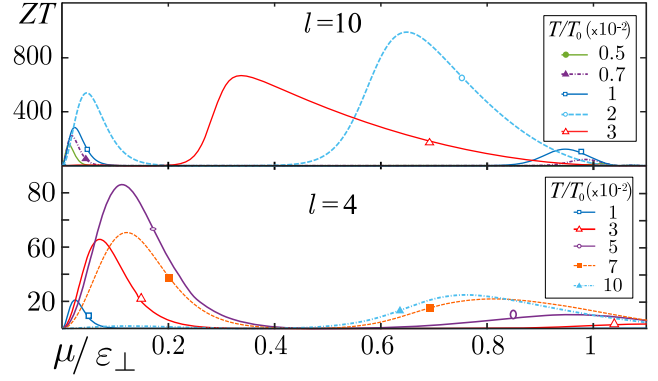


FIG. 5. Figure of merit ZT for two magnetic domains of length $l = 4, 10$, with the perpendicular component of the magnetic moments tilted in $\phi = \pi$. Other details are similar to previous figures.

latter corresponds to a single domain with total length $2L$. On the other hand, for $\phi = \pi$, the energy difference between the peaks is twice the one for $\phi = 0$. Hence, for two domains with $\phi = \pi$, the first peak after the closing of the gap is expected to generate a thermoelectric response with a high figure of merit, similar to that of a Lorentzian function within a range of temperatures larger than in the case of a single ferromagnetic one. For $\mu \sim k_B T$, the thermoelectric response is dominated by the resonance within the gap. This leads to high values of ZT for $k_B T \lesssim 10\gamma$, with γ being the width of the resonance, which depends on the domain length. These details are discussed in the Supplemental Material [70]. For higher temperatures, the transport behavior is dominated by the Heaviside-step function and well-shaped envelopes of the transmission function, and the thermoelectric response is similar to the one discussed for a single domain.

Conclusions.—We have analyzed the transmission function characterizing the coherent transport of electrons in a structure consistent for a pair of helical edge states of a 2D TI coupled to a magnetic island with a magnetic moment having a component perpendicular to the direction of the spin orbit of the TI. We have shown that this setup has the necessary conditions to achieve high performance thermoelectricity. The key is the opening of a gap in the spectrum of the helical edges with a steep increase of the transmission function at the opening of the propagating modes in the spectrum. Depending on the energy range and the configuration of the magnetic domains, the transmission function has features akin to a θ function, as well as with features akin to a δ function, which are known to be optimal for high-power production and figure of merit, respectively. Owing to the resonant states in the gap for two magnetic domains, very large values of the figure of merit, $ZT > 100$, are attained for the heat-engine and refrigeration modes. Our calculations focus on a single pair of edge states, but the currents simply scale in a factor 2 when the pair at the opposite edge is also considered. The range of operation is set by the magnetic gap

ε_{\perp} . For a single domain generating an effective magnetic field of $\sim 1.8\text{--}4$ T [73], we estimate $\varepsilon_{\perp} \sim 1\text{--}2 \times 10^{-4}$ eV, corresponding to reference temperatures $T_0 \sim 1.2\text{--}2.4$ K. According to our work, a device with a length of the magnetic island of $\sim 10L_0$, $L_0 = \varepsilon_{\perp}/\hbar v_F$, operates as a heat engine at high performance ($\sim 75\%$ of the optimal bound) regarding power generation with a figure of merit $ZT \gg 1$ for $T < 0.5T_0$. Taking estimates for the Fermi velocity of the helical edge states in quantum wells of HgTe from Ref. [35], we have $\hbar v_F \sim 0.9$ eV/nm, leading to $L_0 \sim 10\text{--}20$ μm . These parameters are the state of the art of present experimental realizations.

We thank A. Aligia and P. Roura-Bas for carefully reading our manuscript and for the useful comments. We acknowledge support from CONICET, Argentina. We are sponsored by Grant No. PIP-RD 20141216-4905 of CONICET, by Grants No. PICT-2014-2049 and No. PICT-2017-2726 from Argentina, and by the Alexander von Humboldt Foundation, Germany (L. A.).

-
- [1] F. Giazotto, T. T. Heikkilä, A. Luukanen, A. M. Savin, and J. P. Pekola, Opportunities for mesoscopics in thermometry and refrigeration: Physics and applications, *Rev. Mod. Phys.* **78**, 217 (2006).
- [2] G. Benenti, G. Casati, K. Saito, and R. S. Whitney, Fundamental aspects of steady-state conversion of heat to work at the nanoscale, *Phys. Rep.* **694**, 1 (2017).
- [3] G. Granger, J. P. Eisenstein, and J. L. Reno, Observation of Chiral Heat Transport in the Quantum Hall Regime, *Phys. Rev. Lett.* **102**, 086803 (2009).
- [4] S.-G. Nam, E. H. Hwang, and H.-J. Lee, Thermoelectric Detection of Chiral Heat Transport in Graphene in the Quantum Hall Regime, *Phys. Rev. Lett.* **110**, 226801 (2013).
- [5] L. Arrachea and E. Fradkin, Chiral heat transport in driven quantum Hall and quantum spin Hall edge states, *Phys. Rev. B* **84**, 235436 (2011).
- [6] S. Jezouin, F. D. Parmentier, A. Anthore, U. Gennser, A. J. Cavanna, and F. Pierre, Quantum limit of heat flow across a single electronic channel, *Science* **342**, 601 (2013).
- [7] A. Cappelli, M. Huerta, and G. Zemba, Thermal transport in chiral conformal theories and hierarchical quantum Hall states, *Nucl. Phys.* **B636**, 568 (2002).
- [8] E. Grosfeld and S. Das, Probing the Neutral Edge Modes in Transport across a Point Contact via Thermal Effects in the Read-Rezayi Non-Abelian Quantum Hall States, *Phys. Rev. Lett.* **102**, 106403 (2009).
- [9] T. Karzig, G. Refael, L. I. Glazman, and F. von Oppen, Energy Partitioning of Tunneling Currents into Luttinger Liquids, *Phys. Rev. Lett.* **107**, 176403 (2011).
- [10] H. Aita, L. Arrachea, C. Naón, and E. Fradkin, Heat transport through quantum Hall edge states: Tunneling versus capacitive coupling to reservoirs, *Phys. Rev. B* **88**, 085122 (2013).
- [11] G. Viola, S. Das, E. Grosfeld, and A. Stern, Thermoelectric Probe for Neutral Edge Modes in the Fractional Quantum Hall Regime, *Phys. Rev. Lett.* **109**, 146801 (2012).
- [12] I. Gurman, R. Sabo, M. Heiblum, V. Umansky, and D. Mahalu, Extracting net current from an upstream neutral mode in the fractional quantum Hall regime, *Nat. Commun.* **3**, 1289 (2012).
- [13] C. Altimiras, H. le Sueur, U. Gennser, A. Cavanna, D. Mailly, and F. Pierre, Tuning Energy Relaxation along Quantum Hall Channels, *Phys. Rev. Lett.* **105**, 226804 (2010).
- [14] V. Venkatachalam, S. Hart, L. Pfeiffer, K. West, and A. Yacoby, Local thermometry of neutral modes on the quantum Hall edge, *Nat. Phys.* **8**, 676 (2012).
- [15] C. Altimiras, H. le Sueur, U. Gennser, A. Anthore, A. Cavanna, D. Mailly, and F. Pierre, Chargeless Heat Transport in the Fractional Quantum Hall Regime, *Phys. Rev. Lett.* **109**, 026803 (2012).
- [16] M. Banerjee, M. Heiblum, A. Rosenblatt, Y. Oreg, D. E. Feldman, A. Stern, and V. Umansky, Observed quantization of anyonic heat flow, *Nature (London)* **545**, 75 (2017).
- [17] D. F. Mross, Y. Oreg, A. Stern, G. Margalit, and M. Heiblum, Theory of Disorder-Induced Half-Integer Thermal Hall Conductance, *Phys. Rev. Lett.* **121**, 026801 (2018).
- [18] A. Aharon-Steinberg, Y. Oreg, and A. Stern, Phenomenological theory of heat transport in the fractional quantum Hall effect, *Phys. Rev. B* **99**, 041302(R) (2019).
- [19] R. Sánchez, B. Sothmann, and A. N. Jordan, Chiral Thermoelectrics with Quantum Hall Edge States, *Phys. Rev. Lett.* **114**, 146801 (2015).
- [20] P. Samuelsson, S. Kheradsoud, and B. Sothmann, Optimal Quantum Interference Thermoelectric Heat Engine with Edge States, *Phys. Rev. Lett.* **118**, 256801 (2017).
- [21] S. Kheradsoud, N. Dashti, M. Misiorny, P. P. Potts, J. Splettstoesser, and P. Samuelsson, Power, efficiency and fluctuations in a quantum point contact as steady-state thermoelectric heat engine, *arXiv:1904.03912*.
- [22] L. Vannucci, F. Ronetti, G. Dolcetto, M. Carrega, and M. Sasseti, Interference-induced thermoelectric switching and heat rectification in quantum Hall junctions, *Phys. Rev. B* **92**, 075446 (2015).
- [23] P. Roura-Bas, L. Arrachea, and E. Fradkin, Enhanced thermoelectric response in the fractional quantum Hall effect, *Phys. Rev. B* **97**, 081104(R) (2018).
- [24] Xiao-Qin Yu, Zhen-Gang Zhu, Gang Su, and A.-P. Jauho, Spincaloritronic Battery, *Phys. Rev. Applied* **8**, 054038 (2017).
- [25] F. Ronetti, L. Vannucci, G. Dolcetto, M. Carrega, and M. Sasseti, Spin-thermoelectric transport induced by interactions and spin-flip processes in two dimensional topological insulators, *Phys. Rev. B* **93**, 165414 (2016).
- [26] S.-Y. Hwang, R. Lopez, M. Lee, and D. Sanchez, Nonlinear spin-thermoelectric transport in two-dimensional topological insulators, *Phys. Rev. B* **90**, 115301 (2014).
- [27] P.-H. Chang, M. Saeed Bahramy, N. Nagaosa, and B. K. Nikolic, Giant thermoelectric effect in graphene-based topological insulators with nanopores, *Nano Lett.* **14**, 3779 (2014).

- [28] D. G. Rothe, E. M. Hankiewicz, B. Trauzettel, and M. Guigou, Spin-dependent thermoelectric transport in HgTe/CdTe quantum wells, *Phys. Rev. B* **86**, 165434 (2012).
- [29] P. Roura-Bas, L. Arrachea, and E. Fradkin, Helical spin thermoelectrics controlled by a side-coupled magnetic quantum dot in the quantum spin Hall state, *Phys. Rev. B* **98**, 195429 (2018).
- [30] D. Sanchez, R. Sanchez, R. Lopez, and B. Sothmann, Nonlinear chiral refrigerators, *Phys. Rev. B* **99**, 245304 (2019).
- [31] A. Mani and C. Benjamin, Helical thermoelectrics and refrigeration, *Phys. Rev. E* **97**, 022114 (2018).
- [32] C. L. Kane and E. J. Mele, Z_2 Topological Order and the Quantum Spin Hall Effect, *Phys. Rev. Lett.* **95**, 146802 (2005).
- [33] C. L. Kane and E. J. Mele, Quantum Spin Hall Effect in Graphene, *Phys. Rev. Lett.* **95**, 226801 (2005).
- [34] B. A. Bernevig, T. L. Hughes, and S.-C. Zhang, Quantum spin Hall effect and topological phase transition in HgTe quantum wells, *Science* **314**, 1757 (2006).
- [35] M. König, S. Wiedmann, C. Brüne, A. Roth, H. Buhmann, L. W. Molenkamp, X.-L. Qi, and S.-C. Zhang, Quantum spin Hall insulator state in HgTe quantum wells, *Science* **318**, 766 (2007).
- [36] A. Roth, C. Brüne, H. Buhmann, L. W. Molenkamp, J. Maciejko, X.-L. Qi, and S.-C. Zhang, Nonlocal transport in the quantum spin Hall state, *Science* **325**, 294 (2009).
- [37] C. Brüne, A. Roth, H. Buhmann, E. M. Hankiewicz, L. W. Molenkamp, J. Maciejko, X.-L. Qi, and S.-C. Zhang, Spin polarization of the quantum spin Hall edge states, *Nat. Phys.* **8**, 485 (2012).
- [38] B. J. van Wees, H. van Houten, C. W. J. Beenakker, J. G. Williamson, L. P. Kouwenhoven, D. van der Marel, and C. T. Foxon, Quantized Conductance of Point Contacts in a Two-Dimensional Electron Gas, *Phys. Rev. Lett.* **60**, 848 (1988).
- [39] H. van Houten, L. W. Molenkamp, C. W. J. Beenakker, and C. T. Foxon, Thermoelectric properties of quantum point contacts, *Semicond. Sci. Technol.* **7**, B215 (1992).
- [40] M. Büttiker, Quantized transmission of a saddle-point constriction, *Phys. Rev. B* **41**, 7906 (1990).
- [41] J. Strunz, J. Wiedenmann, C. Fleckenstein, L. Lunczer, W. Beugeling, V. L. Müller, P. Shekhar, N. Traverso Ziani, S. Shamim, J. Kleinlein, H. Buhmann, B. Trauzettel, and L. W. Molenkamp, Interacting topological edge channels, [arXiv:1905.08175](https://arxiv.org/abs/1905.08175).
- [42] F. Dolcini, Full electrical control of charge and spin conductance through interferometry of edge states in topological insulators, *Phys. Rev. B* **83**, 165304 (2011).
- [43] P. Virtanen and P. Recher, Dephasing of spin and charge interference in helical Luttinger liquids, *Phys. Rev. B* **83**, 115332 (2011).
- [44] F. Romeo, R. Citro, D. Ferraro, and M. Sassetti, Electrical switching and interferometry of massive Dirac particles in topological insulator constrictions, *Phys. Rev. B* **86**, 165418 (2012).
- [45] B. Rizzo, L. Arrachea, and M. Moskalets, Transport phenomena in helical edge states interferometers, A Green's function approach, *Phys. Rev. B* **88**, 155433 (2013).
- [46] F. Crépin, J. C. Budich, F. Dolcini, P. Recher, and B. Trauzettel, Renormalization group approach for the scattering off a single Rashba impurity in a helical liquid, *Phys. Rev. B* **86**, 121106(R) (2012).
- [47] G. Dolcetto, F. Cavaliere, D. Ferraro, and M. Sassetti, Generating and controlling spin-polarized currents induced by a quantum spin Hall antidot, *Phys. Rev. B* **87**, 085425 (2013).
- [48] K. T. Law, C. Y. Seng, P. A. Lee, and T. K. Ng, Quantum dot in a two-dimensional topological insulator: The two-channel Kondo fixed point, *Phys. Rev. B* **81**, 041305(R) (2010).
- [49] T. Posske, C.-X. Liu, J. C. Budich, and B. Trauzettel, Exact Results for the Kondo Screening Cloud of Two Helical Liquids, *Phys. Rev. Lett.* **110**, 016602 (2013).
- [50] B. Probst, P. Virtanen, and P. Recher, Controlling spin polarization of a quantum dot via a helical edge state, *Phys. Rev. B* **92**, 045430 (2015).
- [51] B. Rizzo, A. Camjayi, and L. Arrachea, Transport in quantum spin Hall edges in contact to a quantum dot, *Phys. Rev. B* **94**, 125425 (2016).
- [52] G. D. Mahan and J. O. Sofo, The best thermoelectric, *Proc. Natl. Acad. Sci. U.S.A.* **93**, 7436 (1996).
- [53] G. Benenti, K. Saito, and G. Casati, Thermodynamic Bounds on Efficiency for Systems with Broken Time-Reversal Symmetry, *Phys. Rev. Lett.* **106**, 230602 (2011).
- [54] R. S. Whitney, Most Efficient Quantum Thermoelectric at Finite Power Output, *Phys. Rev. Lett.* **112**, 130601 (2014).
- [55] R. S. Whitney, Finding the quantum thermoelectric with maximal efficiency and minimal entropy production at given power output, *Phys. Rev. B* **91**, 115425 (2015).
- [56] M. Josefsson, A. Svilans, A. M. Burke, E. A. Hoffmann, S. Fahlvik, C. Thelander, M. Leijnse, and H. Linke, A quantum-dot heat engine operating close to the thermodynamic efficiency limits, *Nat. Nanotechnol.* **13**, 920 (2018).
- [57] P. A. Erdman, F. Mazza, R. Bosisio, G. Benenti, R. Fazio, and F. Taddei, Thermoelectric properties of an interacting quantum dot-based heat engine, *Phys. Rev. B* **95**, 245432 (2017).
- [58] D. Prete, P. A. Erdman, V. Demontis, V. Zannier, D. Ercolani, L. Sorba, F. Beltram, F. Rossella, F. Taddei, and S. Roddaro, Thermoelectric conversion at 30K in InAs/InP nanowire quantum dots, *Nano Lett.* **19**, 3033 (2019).
- [59] B. Dutta, J. T. Peltonen, D. S. Antonenko, M. Meschke, M. A. Skvortsov, B. Kubala, J. König, C. B. Winkelmann, H. Courtois, and J. P. Pekola, Thermal Conductance of a Single-Electron Transistor, *Phys. Rev. Lett.* **119**, 077701 (2017).
- [60] O. Entin-Wohlman, Y. Imry, and A. Aharony, Enhanced performance of joint cooling and energy production, *Phys. Rev. B* **91**, 054302 (2015).
- [61] D. Pérez Daroca, P. Roura-Bas, and A. A. Aligia, Enhancing of nonlinear thermoelectric response of a correlated quantum dot in the Kondo regime by asymmetrically coupling to the leads, *Phys. Rev. B* **97**, 165433 (2018).
- [62] D. B. Karki and M. N. Kiselev, Exceeding quantum upper bound of power production in nano devices: Effects of resonance scattering and strong electron interactions, [arXiv:1906.00724](https://arxiv.org/abs/1906.00724).

- [63] Q. Meng, S. Vishveshwara, and T. L. Hughes, Spin-transfer torque and electric current in helical edge states in quantum spin Hall devices, *Phys. Rev. B* **90**, 205403 (2014).
- [64] L. Arrachea and F. von Oppen, Nanomagnet coupled to quantum spin Hall edge: An adiabatic quantum motor, *Physica (Amsterdam)* **74E**, 596 (2015).
- [65] P. G. Silvestrov, P. Recher, and P. W. Brouwer, Noiseless manipulation of helical edge state transport by a quantum magnet, *Phys. Rev. B* **93**, 205130 (2016).
- [66] L. Fu and C. L. Kane, Josephson current and noise at a superconductor/quantum-spin-Hall-insulator/superconductor junction, *Phys. Rev. B* **79**, 161408(R) (2009).
- [67] M. Houzet, J. S. Meyer, D. M. Badiane, and L. I. Glazman, Dynamics of Majorana States in a Topological Josephson Junction, *Phys. Rev. Lett.* **111**, 046401 (2013).
- [68] F. Crépin, B. Trauzettel, and F. Dolcini, Signatures of Majorana bound states in transport properties of hybrid structures based on helical liquids, *Phys. Rev. B* **89**, 205115 (2014).
- [69] R. Bustos-Marun, G. Refael, and F. von Oppen, Adiabatic Quantum Motors, *Phys. Rev. Lett.* **111**, 060802 (2013).
- [70] See Supplemental Material at <http://link.aps.org/supplemental/10.1103/PhysRevLett.123.186801> for details on the behavior of the maximum power for the heat engine and the figure of merit of the reference transmission functions.
- [71] R. Jackiw and C. Rebbi, Solitons with fermion number, *Phys. Rev. D* **13**, 3398 (1976).
- [72] W. P. Su, J. R. Shrieffer, and A. J. Heeger, Soliton excitations in polyacetylene, *Phys. Rev. B* **22**, 2099 (1980).
- [73] G. Scheunert, O. Heinonen, R. Hardeman, A. Lapicki, M. Gubbins, and R. M. Bowman, A review of high magnetic moment thin films for microscale and nanotechnology applications, *Appl. Phys. Rev.* **3**, 011301 (2016).